Available online at www.sciencedirect.com

Chemical Engineering Research & Design

DOI : 10.1016/j.cherd.2015.09.020

www.elsevier.com/locate/cherd

Influence of nozzle design on the performance of a partial combustion lance: A CFD study

Woon Phui Law[1] and Jolius Gimbun[1,2,†]

[1] *Faculty of Chemical and Natural Resources Engineering, Universiti Malaysia Pahang, Pahang 26300, Malaysia*
[2] *Centre of Excellence for Advanced Research in Fluid Flow, Universiti Malaysia Pahang, Pahang 26300, Malaysia*

Abstract

This paper presents a computational fluid dynamics (CFD) simulation of a partial combustion lance (PCL) aiming to evaluate the effect of nozzle design on its performance. Four turbulence models, namely, standard *k-ε* (SKE), realisable *k-ε* (RKE), renormalised (RNG) *k-ε* and Reynolds stress model (RSM) were used. The combustion process was modelled using the species transport model, whereas the heat transfer was calculated by considering a combined convection-radiation boundary condition. The best CFD prediction was obtained using the second-order discretisation, standard pressure, unsteady solver and RSM with a 6% deviation from the experimental data. The modified nozzle design shows increases in excess of 45% of the peak combustion temperature in the PCL. The findings from this work may be useful for design retrofits of a PCL.

Keywords: CFD; modelling strategy; unsteady RANS; turbulence; combustion; nozzle design

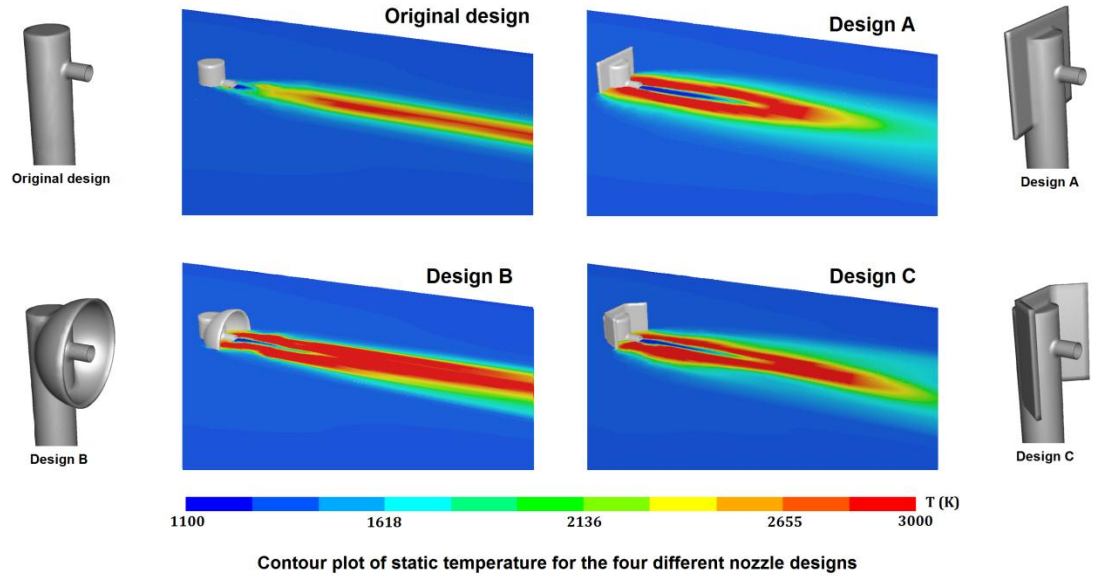

Temperature profile of syngas combustion from different nozzle design

*Corresponding author: jolius@ump.edu.my (J. Gimbun)

Citation information:
Woon Phui Law, Jolius Gimbun, Influence of nozzle design on the performance of a partial combustion lance: A CFD study, Chemical Engineering Research & Design, ISSN 0263-8762, http://dx.doi.org/10.1016/j.cherd.2015.09.020

1. Introduction

Partial combustion of syngas is often used to produce high-quality metallic iron in a steel processing plant. Partial combustion lance (PCL) is used to increase the temperature of syngas, in which extreme operating temperature (more than 1193 K) and pressure (more than 55 kPa) are needed for the reduction process from iron ore to metallic iron. In most cases, the partial combustion device suffers from low combustion efficiency, poor heat transfer, pollutant formation and particle deposition mostly due to weak design configuration and non-optimum operating condition. The nozzle plays an important role in the fuel-oxidant mixing in the combustion system and hence may significantly affect the PCL performance. Earlier, we demonstrated that higher oxygen flowrate enhances the combustion reaction and thus, increases the peak combustion temperature of the PCL. However, the present work focuses on the effect of the nozzle design on PCL performance.

The effect of nozzle or fluid injector geometry on combustion performance had been investigated extensively by many researchers in various applications. Their works mainly focused on parameters such as the nozzle diameter (Athayde et al., 2012; Zhang et al., 2014a), nozzle shape (Benajes et al., 2004; Som et al., 2011; Taskiran and Ergeneman, 2014; Barik et al., 2015), the angle between nozzles (Gao et al., 2009) and number of nozzles (Barik et al., 2015). Athayde et al. (2012) studied the effect of nozzle diameter on the flame pattern in the combustion chamber. They reported that a large fuel injector tends to reduce the inlet velocity, and thus producing unstable and highly deflected flames. This resulted to poor combustion, increased dust deposition and in some cases, cause damage to the chamber walls. Benajes et al. (2004) and Som et al. (2011) made comparisons between the cylindrical and conical nozzles in the diesel engine. Benajes et al. (2004) concluded that cylindrical nozzle is the best nozzle type for diesel combustion, because it gives higher cavitation and Reynolds number leading to better combustion compared to the conical nozzle. However, Som et al. (2011) presented a contradicting finding. They reported that conical nozzle produces better pre-mixed combustion, but has a higher soot production than that of a cylindrical nozzle. Gulati et al. (2009) studied the effect of various nozzle types on local heat transfer distribution. Therectangular nozzle produced the highest local Nusselt number distribution in comparison to the circular and square nozzles. The highest pressure loss was observed for rectangular nozzle while the lowest pressure loss was observed for the circular nozzle, although all nozzles showed almost identical average Nusselt number distribution. Taskiran and Ergeneman (2014) investigated the effect of four different nozzle shapes on the flame pattern using the SKE turbulence model. They found that a divergent nozzle with sharp inlet has a shorter flame lift-off length and lower flame temperature due to the disruptive effect of nozzle divergence in a same manner as the diffuser. Whereas, a comparable flame was observed for another three nozzle types (convergent nozzle with rounded inlet, straight nozzle with sharp inlet and straight nozzle with rounded inlet). It should be noted that the nozzle comparison conducted by Gulati et al. (2009) and Taskiran and Ergeneman (2014) were not made based on a similar nozzle size, which may affect the interpretation of their study. Barik et al. (2015) compared the performance of circular and non-circular nozzles on the entrainment rate of air. A higher mixing and entrainment rate of air was observed in a non-circular nozzle compared to a circular nozzle. They also reported an improved entrainment rate using multiple nozzles compared to a single nozzle. Thus, it can be concluded from the previous works that the nozzle geometry may affect the combustion performance and hence detailed study of its design is a matter of interest. In the case of PCL, syngas-oxygen mixing depends mainly on the nozzle geometry. Thus, a poor PCL design can significantly affect the performance of the combustion process. Therefore, three modified nozzles (i.e., flat surface, semi-sphere hollow and bended wingtip) were proposed for the present study.

Fluid flow in a PCL has been widely studied experimentally and numerically by numerous researchers. Early studies on the fluid flow measurements in a combustion unit were performed using Schlieren photography (Bradley and Hundy, 1971) and hot-wire anemometry (Miller et al., 1946). In the recent years, advanced techniques such as particle image velocimetry (PIV), which provides detailed visualisation on the flow pattern were also used (Zhang et al., 2014b). However, PIV measurement is impractical on opaque wall, which most combustion chambers are built with. Furthermore, it is potentially dangerous to employ a PIV measurement on large industrial-scale PCL operating at temperatures above 1000 K. Therefore, a CFD technique capable of providing comprehensive data on the fluid flow, reaction, heat and mass transfer inside the PCL was employed in this work.

Most of the previous CFD works on the combustion unit use k-ε based models (i.e., SKE, RKE and RNG) owing to its robustness. Moreover, the k-ε based models converge easily and have relatively lower computational cost.

However, there is limited literature background on the comparison between the prediction of different turbulence models. In addition to that, the solution was often assumed to be steady-state to reduce the complexity and computational time (Abbasi Khazaei, 2010). Hence, although the general trend of the flow was correctly predicted, the prediction accuracy still needs further refinement. There is also a limited study on the effect of the modelling strategy such as discretisation, pressure interpolation scheme, solver and turbulence models on the prediction accuracy for PCLs. Furthermore, some numerical studies did not perform validations with experimental data (e.g., Abbasi Khazaei, 2010). A well-developed numerical model for PCL is important as they can significantly affect the accuracy and reliability of CFD studies. Hence, this work aims to develop a modelling strategy to predict the temperature and velocity profile in a PCL. The CFD prediction was compared with the experimentally measured temperature (Zain et al., 2011) and velocity profile (Lourenco and Shih, 1993) for validation purpose. Once validated, the model was used to study the effect of nozzle design on the temperature profile in the PCL. According to Galletti et al. (2007), modified air injection nozzle design improved fluid motion and decreased pollutant emissions. However, the fluid flow and reaction mechanism involved has not been elucidated and this is part of the aim of this work.

2. Geometry and computational grid

A three-dimensional horizontal cylindrical PCL fitted with two oxygen lances and nozzles, as shown in Fig. 1, was prepared using GAMBIT 2.4.6. The cylindrical PCL is 6.35 m in length and has a diameter of 1.266 m. Each oxygen lance has a length of 0.483 m and a diameter of 0.06 m, whereas the nozzle has a length of 0.03 m and a diameter of 0.022 m. Both oxygen lances were installed 1.35 m from the PCL inlet. The distance between both oxygen lances is 0.30 m. Nozzles are attached 0.039 m from the lances. The fuel gas is injected into PCL at 1203 K and 118 m/s, while pure oxygen is injected at 300 K and 70 m/s through the nozzles. The PCL wall is made of 0.03 m thick steel with a convective heat transfer coefficient of 0.5 $W/m^2 \cdot K$. The geometry of the PCL in this work is similar to the one studied by Zain et al. (2011) in our previous work. The geometry was meshed using unstructured meshes, i.e., tetrahedral and hexahedral meshes, which were then converted into a polyhedra mesh. Higher grid densities (finer cells) were created near the oxygen lances and flame region, while the rests of the PCL regions were meshed with coarser cells. About 418k nodes were employed for the whole PCL domain.

The PCL in this work is a part of a Tenova HYL direct reduction process which was installed between the process gas heater and oxide removal reactor. The gas composition at the PCL inlet was measured using a micro gas chromatography (Agilent GC 3000) and the temperature was measured using a type-K thermocouple. A molecular sieve column was used for the analysis of hydrogen (H_2), methane (CH_4), oxygen (O_2), nitrogen (N_2) and carbon monoxide (CO) at 368 K, whereas the Plot U column was used for the analysis of carbon dioxide (CO_2) at 373 K. A high purity (over 99.99%) helium (He) gas was used as the carrier gas. A type-K thermocouple was chosen with

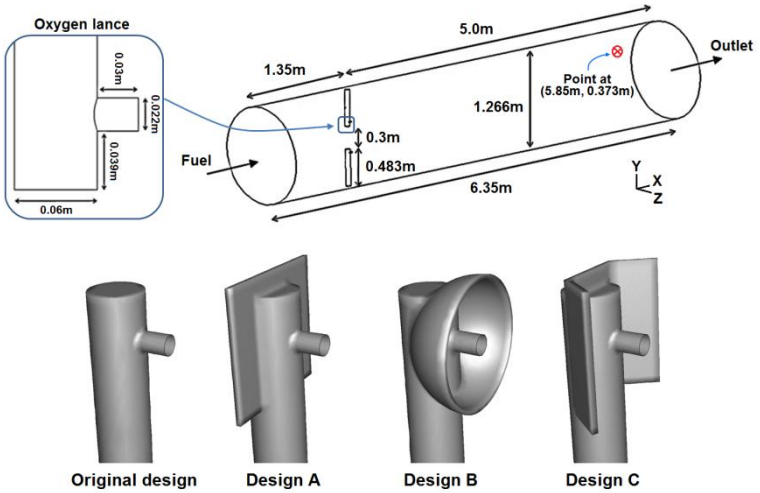

Fig. 1 - A schematic of PCL and oxygen lance geometry.

regards to its favourable use in oxidising environments and has a measurement range of 73.15 K to 1533.15 K. The type-K thermocouple has a tolerance of ±2.5 K at the range of temperature between 233.15 K to 606.15 K and ±0.0075T K at the range of temperature between 606.15 K to 1473.15 K. The thermocouple was installed at a position of 5.85 m after the inlet, just before the oxide removal reactor. Due to the opaque PCL wall design and the fabrication cost, only one temperature measurement point is allowed. Besides, the outlet of the PCL is directly connected to the inlet of the reactor, which further complicates the experiment. Nevertheless, the CFD prediction was compared with the experimentally measured velocity profile by Lourenco and Shih (1993) to ensure the model chosen and the grid prepared are sufficient to capture the flow feature past the cylindrical oxygen lance. Other aspects such as the use of higher-order discretisation and a proper grid dependency analysis were performed to minimise the simulation error. In addition, the mass balance between the inlet and outlet flow was checked to ensure solution convergence.

The original nozzle design is wingless, which leads to poor turbulent mixing and low flame intensity, thus, modification of the nozzle design was studied. Three modified nozzle designs were proposed for evaluation, namely design A, B and C. A simple flat surface and a semi-sphere hollow shape were introduced in design A and B, respectively. Meanwhile, design C is a bended wingtip commonly used in the industry. The cross-sectional areas of the nozzle wings were set to a constant for all designs to give a fair comparison between each design. The influence of modified nozzle designs on the performance of the PCL was evaluated. A sketch of the original and three modified nozzle designs are shown in Fig. 1.

3. CFD model

3.1 Turbulence modelling

A combination of intense chemical reaction and high velocity produced a highly turbulent fluid flow in the PCL. In turbulent flows, velocity component and pressure fluctuate chaotically, which cause transport quantities, such as mass, momentum and energy to fluctuate as well. Reynolds-averaged Navier-Stokes (RANS) based turbulence model is most commonly used for turbulent modelling in many practical engineering applications due to its low computational demand and robustness. RANS model decomposed the real variables (instantaneous) into mean and fluctuating components as follows:

$$\phi = \bar{\phi} + \phi' \tag{1}$$

where ϕ is a scalar variable, $\bar{\phi}$ is the mean component and ϕ' is the fluctuating component. The Eq. (1) is substituted into the mean continuity and momentum equations to form the RANS equations. The mean RANS equations are given by:

$$\frac{\partial \bar{u}_i}{\partial x_i} = 0 \tag{2}$$

$$\rho \frac{\partial \bar{u}_i}{\partial t} + \rho \bar{u}_j \frac{\partial \bar{u}_i}{\partial x_j} = \rho \bar{f}_i + \frac{\partial}{\partial x_j}\left[-\bar{p}\delta_{ij} + 2\mu \bar{S}_{ij} - \rho \overline{u_i' u_j'} \right] \tag{3}$$

where $\bar{u}_i$ is mean velocity, ρ is fluid density, $\bar{f}_i$ is external forces, $\bar{p}$ is mean pressure, μ is fluid viscosity, $\bar{S}_{ij} = 0.5\left(\partial \bar{u}_i / \partial x_j + \partial \bar{u}_j / \partial x_i\right)$ is the mean strain tensor rate and $-\rho \overline{u_i' u_j'}$ is the Reynolds stresses tensor.

The SKE has been a workhorse for many practical turbulence flow analysis for some time owing to its robustness and simplicity. The SKE model is a simple yet robust two-equation turbulence model to account for both kinetic energy and dissipation rate. The SKE is known to perform poorly for flows containing large adverse pressure gradients, as well as in cases such as unconfined flows, curved boundary layers and rotating flows. Shih et al. (1995) introduced the RKE model to improve the SKE prediction as the strengths and weaknesses of the SKE model has become known. The RKE model is a substantial improvement over the SKE, as it considers flow features such as strong streamline curvature, vortices and rotation. The RKE differs from the SKE model in two important ways:

first, it has a new formulation for turbulent viscosity and second, it employs a new transport equation for the dissipation rate. RKE still has a similar equation for μ_t as SKE, but C_μ is no longer a constant and instead is a function of velocity gradients, which consider the positivity of normal stresses ($\overline{u_i^2} \geq 0$) and Schwarz's inequality for shear stress ($\overline{(u_i u_j)}^2 \leq \overline{u_i^2}\ \overline{u_j^2}$). The Schwarz inequality for shear stresses in the *k-ε* model can be violated when the mean strain rate is large, but it can be eliminated by having a variable C_μ (Fluent Inc, 2006). RNG *k-ε* was derived from a renormalised group theory by Yakhot and Orzag (1986). In RNG *k-ε* model, the small-scale eddies are eliminated and the transport coefficient is renormalised. RNG *k-ε* consists an analytical equation for turbulent Prandtl number (Pr_t) and an additional term (R_ε) in the turbulent dissipation rate transport equation to account for the interaction between turbulence dissipation and mean shear. The additional term gives a slight reduction of dissipation rate and the effective viscosity, which improved predictions for rapidly strained flow and streamline curvature (Yakhot and Orzag, 1986). Nevertheless, all three *k-ε* variant use a similar assumption for turbulent viscosity (Boussinesq hypothesis), which led to a major shortfall of these models.

The RSM model abandoned the isotropic eddy viscosity assumption by taking into account the effects of streamline curvature, anisotropy, rotation and rapid changes in strain rate in a more rigorous manner than the one- and two-equation models. Hence, the RSM has the potential to give more accurate predictions for complex flows (Andersson et al., 2012). Simulation using RSM model requires a relatively higher computational cost to solve the seven additional transport equations for three-dimensional problem. In addition, RSM simulation at higher orders of discretisation for the combustion system is challenging, as the solution is prone to divergence (Gimbun et al., 2005). Therefore, RSM simulation in this work was initially performed using the first-order upwind scheme without activating the species transport and the under-relaxation factor for turbulent stress was reduced to 0.3. The linear pressure-strain was used throughout this work. The species transport (reaction) and the second-order upwind scheme was enabled sequentially once the simulation stabilised (characterised by flatter overall residuals).

3.2 Heat transfer modelling

The radiation and convection are the dominant heat transfer mechanisms in PCL. Earlier works by Abbasi Khazaei et al. (2010) and Park et al. (2013) show that in a conventional combustion process, radiation is a dominant heat transfer mode in a combustor, accounting for 96% of the total heat transfer while only 4% is resulted from convective heat transfer. In a PCL, both convective and radiative heat transfer occurs simultaneously (Welty et al., 2001), whereby the rate of total heat transfer is given by:

$$\dot{Q} = \dot{Q}_C + \dot{Q}_R \tag{4}$$

where $\dot{Q}_C$ is the rate of heat transfer due to convection and $\dot{Q}_R$ is the rate of heat transfer due to radiation. The rate of convective heat transfer (Gubba et al., 2012) is given by:

$$\dot{Q}_C = h\left(T_g - T_s\right) \tag{5}$$

where *h* is convective heat transfer coefficient, T_g and T_s are temperature of gas and wall surface, respectively. The convective heat transfer coefficient, *h*, in turbulent flow is computed using Nusselt number (Incropera and DeWitt, 2000):

$$Nu = \frac{hx}{k} \tag{6}$$

$$Nu = 0.027\,\mathrm{Re}^{0.8}\,\mathrm{Pr}^{1/3}\left(\frac{\mu}{\mu_s}\right)^{0.14} \tag{7}$$

where *x* is the characteristic length of the boundary layer, *k* is the thermal conductivity of gas, *Re* is Reynolds

number, *Pr* is Prandtl number ($\mathrm{Pr} = \mu c_p / k$), μ is gas viscosity of bulk fluid, μ_s is the gas viscosity at the wall surface of PCL and c_p is specific heat capacity of gas. Nusselt number, *Nu*, was obtained using the Sieder-Tate correlation (Sieder and Tate, 1936). Sieder-Tate correlation provides more accurate prediction since it accounts for the viscosity gradient due to the large difference between the gas temperature and the wall surface temperature. The rate of radiation (Gubba et al., 2012) is given by:

$$\dot{Q}_R = \varepsilon\sigma(T_r^4 - T_s^4) \tag{8}$$

where ε is emissivity of PCL wall, σ is the Stefan-Boltzmann constant, T_r is radiation temperature and T_s is the PCL wall surface temperature.

3.3 Species transport modelling

A PCL mainly involves species transport, heat transfer and turbulent mixing. Interactions between the fuel gas and O_2 affect the flame pattern and reaction intensity, thus may affect the overall performance of the PCL. The chemical reaction during the partial combustion in a PCL is shown in Table 1. Five steps reaction mechanisms and their parameters were defined according to the FLUENT built-in global database (Westbrook and Dryer, 1984). Reactions 1 and 4 are the partial and complete combustion of CH_4, respectively; reactions 2 and 3 are the partial combustion of syngas (CO and H_2, respectively) and reaction 5 represents the CO_2 dissociation. All reactions are exothermic except for the CO_2 dissociation in reaction 5. The composition of the inlet gas is given in Table 2.

The mass-averaged transport equation as follows:

$$\frac{\partial}{\partial x_j}(\rho \bar{u}_j \bar{Y}_i) = -\frac{\partial^2}{\partial x_i^2}\left[\left(\rho D_{i,m} + \frac{\mu_t}{Sc_t}\right)\bar{Y}_i\right] + R_i + S_i \tag{9}$$

where $\bar{u}_j$ is mass-averaged velocity of mixture, $\bar{Y}_i$ is the mass fraction, $D_{i,m}$ is a diffusion coefficient for species *i* in the mixture, μ_t is turbulent viscosity and Sc_t is the turbulent Schmidt number which is computed as function of turbulent diffusivity, D_t, as $Sc_t = \mu_t / \rho D_t$. R_i is the net rate of species production by chemical reaction and S_i is the source term responsible for the generation or destruction of the gas species due to the chemical reaction. In this work, partial combustion of syngas was modelled by the combination of the finite rate and eddy dissipation

Table 1 - Parameters for the five chemical reactions.

Reaction number	Chemical reaction	Rate order	Pre-exponential factor	Activation energy (J/kg mol)
1	$CH_4 + 1.5O_2 \rightarrow CO + 2H_2O$	$[CH_4]^{0.7}[O_2]^{0.8}$	5.012×10^{11}	2.0×10^{8}
2	$CO + 0.5O_2 \rightarrow CO_2$	$[CO]^{1}[O_2]^{0.25}$	2.239×10^{12}	1.7×10^{8}
3	$H_2 + 0.5O_2 \rightarrow H_2O$	$[H_2]^{1}[O_2]^{1}$	9.87×10^{8}	3.1×10^{7}
4	$CH_4 + 2O_2 \rightarrow CO_2 + 2H_2O$	$[CH_4]^{0.2}[O_2]^{1.3}$	2.119×10^{11}	2.03×10^{8}
5	$CO_2 \rightarrow CO + 0.5O_2$	$[CO_2]^{1}$	5.0×10^{8}	1.7×10^{8}

Table 2 - Composition of the inlet syngas.

Component	Mass fraction
CH_4	0.132
CO	0.486
CO_2	0.072
H_2	0.154
H_2O	0.029
N_2	0.126

model (EDM), instead of a stiff and expensive eddy dissipation concept (EDC) model. The Damkohler number for the case in this work is 7.65 (fast reaction) which is greater than 1.0 and hence better modelled by EDM. Guessab et al. (2013) reported that finite rate-EDM yielded a good prediction for multiple step reactions problem. The finite rate model calculates the chemical reaction rate according to the Arrhenius equation, where the turbulent mixing effect is negligible. In the EDM, a fast chemical reaction was assumed to be controlled by turbulent mixing. A finite rate-EDM approach includes both Arrhenius and mixing rates, whereby the lower rate from either model will dictate the reaction. The net rate of species production, R_i is modelled as:

$$R_i = M_{w,i} \sum_{r=1}^{N_R} \hat{R}_{i,r} \tag{10}$$

where $M_{w,i}$ is the molecular weight of the combustion species, N_R is total number of reactions, r is reaction and $\hat{R}_{i,r}$ is the Arrhenius chemical reaction rate of species. In the EDM, R_i is modelled according to Magnussen and Hjertager (1977):

$$R_i = v'_{i,r} M_{w,i} A \rho \frac{\varepsilon}{k} \min_R \left(\frac{Y_R}{v'_{R,r} M_{w,R}} \right) \tag{11}$$

$$R_i = v'_{i,r} M_{w,i} A B \rho \frac{\varepsilon}{k} \frac{\sum_p Y_P}{\sum_j^N v''_{j,r} M_{w,j}} \tag{12}$$

where $v'_{R,r}$ and $v''_{j,r}$ are the reactant and product species's stoichiometric coefficients, respectively, A = 4.0 is Magnussen constant for reactant, B = 0.5 is Magnussen constant for product, Y_P and Y_R are the mass fractions of the species in the product and reactant, respectively.

4. Modelling strategy

The CFD simulation was initiated by assuming a uniform X-velocity (70 m/s) inside the whole domain (patched) to facilitate faster convergence, knowing the inlet velocity in the X-direction of 118 m/s. At first, the PCL simulation was performed using a first-order discretisation. The physical properties of fluid (i.e., density, specific heat, thermal conductivity and viscosity) obtained from various sources (Keenan et al., 1983; Touloukian et al., 1970a, 1970b) ranging from 123 K to 2273 K were introduced to the simulation as a piecewise linear function. A higher-order discretisation (i.e., second-order) was enabled later to obtain an accurate prediction. All residuals were set to fall below 1×10^{-5} to ensure a good convergence was achieved for all simulations performed using the steady solver. The CFD prediction was recorded for over 1000 iterations and averaged after a convergence. Meanwhile, the statistical convergence of the velocity, temperature, static pressure and strain rate was monitored for the unsteady simulation because the residual monitoring is not meaningful. Data were recorded for over 1000 time steps and were averaged once a pseudo-steady condition was reached. The standard deviation from the mean of the recorded data is reported as an error bar. The predicted normalised mean velocity profiles were compared with the experimental data from Lourenco and Shih (1993) at different downstream position from the cylindrical oxygen lance. The freestream flow velocity, u_∞ was set to correspond to a subcritical Reynolds number of 3900, to ensure a fair comparison to the measurement by Lourenco and Shih (1993). Meanwhile, the predicted temperature was compared with the experimental data from our previous work (Zain et al., 2011). Zain et al. (2011) reported an experimentally measured temperature of 1293 K at position of 5.85 m from the PCL inlet and 0.373 m from PCL wall as shown in Fig. 1. CFD simulation in this work was performed using six units of HP Z220 workstation with a quad core processor (Xeon 3.2 GHz E3-1225) and eight Gigabytes of RAM. Each CFD case takes about two weeks of iterations to achieve a pseudo-steady solution.

5. Results and discussion

5.1 Model development and validation

In this work, the air flows past an oxygen lance (i.e., the original design) in a PCL at a subcritical Reynolds number of 3900 was compared with the PIV measurement by Lourenco and Shih (1993), because the PCL is a relatively simple geometry whereby the only disturbance to the flow is due to the oxygen lances. The predicted mean velocity profiles using four turbulence models, namely SKE, RKE, RNG k-ε and RSM were compared with the experimental measured data (Lourenco and Shih, 1993).

Fig. 2 showed the normalised mean streamwise and crossflow velocities along the radial position (Z/D) at different axial position (X/D), respectively. The lowest normalised mean streamwise velocity was achieved around the centre region (-0.5 < Z/D < 0.5), just after the cylindrical oxygen lance. Meanwhile, a higher normalised mean streamwise velocity was obtained in the undisturbed flow (-1.5 < Z/D < -0.5 and 0.5 < Z/D < 1.5). No appreciable differences were observed from the prediction using different turbulence models, whereby all models showed fairly good agreement with the experimental data (Lourenco and Shih, 1993). Approximately 26% to 57% deviation between the predicted and experimental measurement was achieved by unsteady SKE, RKE, RNG and RSM in the present work. This finding is considered acceptable compared to the previous CFD works with a similar setup. For instance, Rodi (1997) and Iaccarino et al. (2003) showed deviation up to 305% using steady RANS models, while the unsteady RANS models showed lower errors ranging from 31% to 118% (Iaccarino et al., 2003; Muddada and Patnaik, 2010; Unal et al., 2010). Larger errors from previous works may be attributed to inadequate grid resolution,

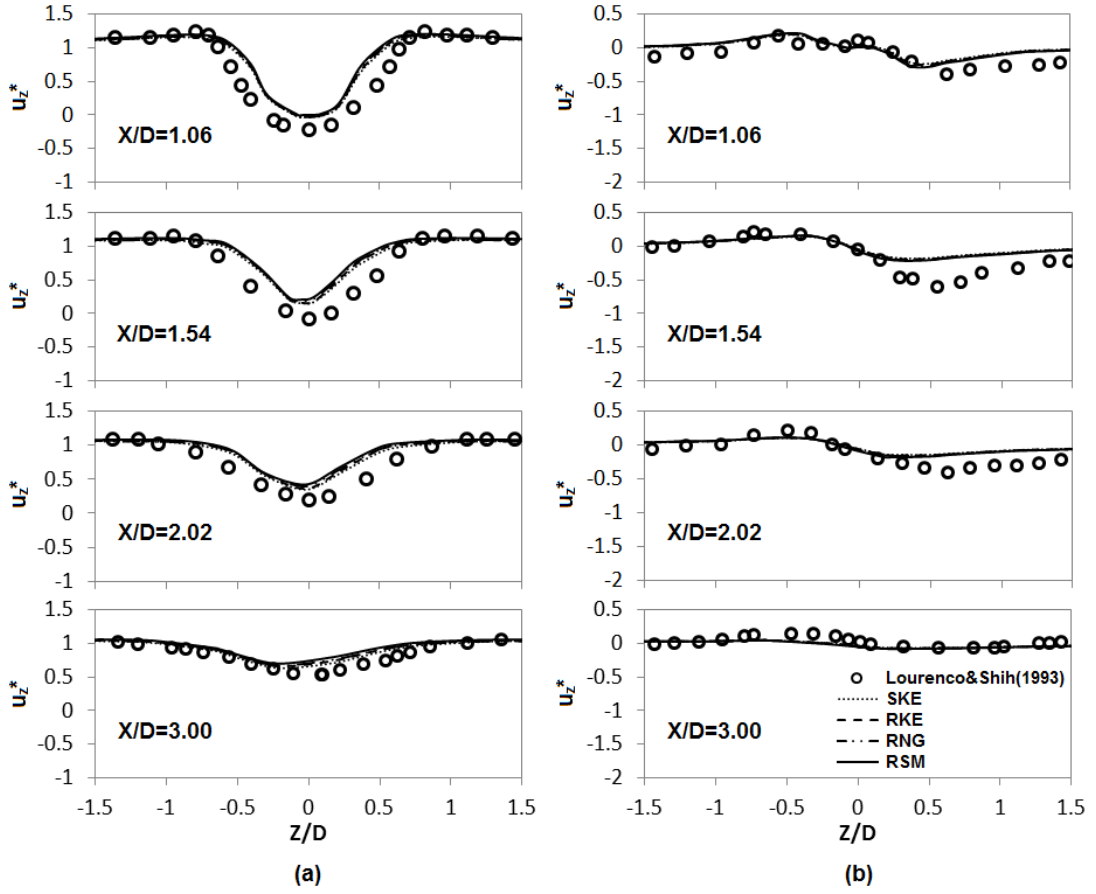

Fig. 2 - CFD prediction on flow past the cylindrical oxygen lance, (a) normalised mean streamwise velocity, $u_x^* = u_x/u_\infty$; and (b) normalised mean crossflow velocity, $u_z^* = u_z/u_\infty$ along the radial position at different X/D. Data points adopted from Lourenco and Shih (1993).

numerical models and complex flows, since the fluid flow past a cylinder is highly unstable, where an extended separation layers and unstable turbulent wake flows existed around the cylinder. In this work, a sufficient grid refinement (y^+ ~ 2 to 30) was made around the cylindrical lances and in the wake region. The discrepancy between the CFD prediction and experimental data may be due to the minor differences in the case setup. In this work, the cylindrical oxygen lances are attached inside a circular combustion channel, whereas the measurement by Lourenco and Shih (1993) was performed in an unconfined infinite cylinder. Nevertheless, the difference in the setup is not thought to affect the prediction on the immediate vicinity of the oxygen lance. The studies performed by Beaudan and Moin (1994) and Kravchenko and Moin (2000) reported that the accuracy of a prediction is significantly affected by the grid resolution. An inadequate grid resolution (too coarse) may cause poor prediction. The predicted velocity in this work is in fairly good agreement with the PIV measurement, which implies that the correct modelling approach was used and the grid resolution of the oxygen lance is sufficient to resolve the air flow feature. In this work, the grid resolution at the nozzle was set at 0.005 m and 0.008 m at the oxygen lance surface, respectively. Twelve grid cells were employed across the diameter of the oxygen lance to resolve the wake flow. An adequate grid resolution is vital to ensure the influence of the nozzle geometry modification is well captured. A similar grid resolution was used in all cases to ensure correct prediction of the flow feature past the oxygen lance. In addition, the turbulent structure for SKE, RKE, RNG and RSM represented by lambda-2 criterion at λ_2 = -400 and λ_2 = -5000 is shown in Fig. 3. Lambda-2 is a negative second eigen value of $S_{ik}S_{kj}+\Omega_{ik}\Omega_{kj}$, where the strain tensor is given as $S_{ij}=0.5(du_i/dx_j+du_j/dx_i)$ and vorticity tensor is $\Omega_{ij}=0.5(du_i/dx_j-du_j/dx_i)$, respectively. S is the symmetric component of the gradient velocity tensor related to the amount of stretching and folding that derives mixing to occur. Ω is the antisymmetric component of the gradient velocity tensor, which determines the vorticity motion. Lambda-2 is used to reflect various scales and structure of turbulent flow from a three-dimensional velocity field. This criterion had been employed by many researchers for various cases such as in aerodynamics (Brett et al., 2010), rotation of turbine blade (Nicolle et al., 2010) and aquatic locomotion (Kazakidi et al., 2015). In Fig. 3, smaller scale eddies exist around the cylindrical oxygen lance, while larger scale eddies were present just after the oxygen lance. These findings indicated that the prediction using RSM capture larger and longer scale of turbulent eddies, whereas poorer flow feature was presented by SKE, RKE and RNG. In this work, RSM yielded better flow feature prediction than the other three turbulence models in Fig. 3, although Fig. 2 showed no appreciable difference between the model tested.

A steady simulation of the fluid flow in a PCL was studied in our previous work (Law and Gimbun, 2015). The finding showed that a combination of the second-order upwind and standard pressure schemes yielded the best agreement with the experimental data (Zain et al., 2011). This is attributed to the numerical diffusion typically associated with the first-order scheme, whereas the QUICK scheme is superior only for structured mesh, while the second-order scheme is sufficient for most CFD solutions (Andersson et al., 2012). The prediction using four pressure interpolation schemes (i.e., standard, second-order, linear and PRESTO) did not show any significant difference. Although, the standard pressure interpolation scheme showed a closer agreement with the experimental data (Zain et al., 2011) while the PRESTO produced a poorer prediction.

The effect of the solver on the prediction accuracy of the temperature in the PCL was performed using the second-order upwind scheme, standard pressure interpolation scheme and SKE turbulence model. It was found that the unsteady solver yielded a similar mean error with the steady solver (5.86%) although the standard deviation for the unsteady solver is much smaller (Table 3). Earlier, Benim et al. (2004) reported that no significant difference between the transient and steady simulation on the wall heat flux prediction in a turbulent pipe flow. Although several authors claimed that prediction using unsteady RANS is somewhat better than the steady RANS. For instance, Iaccarino et al. (2003) reported that the steady RANS over-predicted the recirculation flow in the wake of the cylinder. Moreover, the unsteady RANS model showed a better agreement with the experimental velocity profile than the steady RANS model. Similarly, Lian and Merkle (2011) showed that the time-averaged unsteady simulation yielded a more accurate prediction than steady simulation on the wall heat flux in a combustion chamber. Piomelli (2014) also reported that the steady RANS is unable to capture the flow feature over a circular cylinder, meanwhile unsteady RANS successfully captured turbulent eddies. In our recent work (Gimbun et al., 2015), we found that unsteady RANS yielded a better prediction on axial velocity than that of steady RANS although the difference is marginal. Generally, most of the previous work concluded that unsteady RANS resolved the fluid flow better than the steady RANS, although the difference in prediction accuracy is not substantial. In this case, either solvers may

be used with no appreciable differences, although the unsteady solver may give a more accurate prediction. Nevertheless, the unsteady solver was employed for the remainder of this work due to its lower standard deviation.

In this work, four turbulence models, i.e., SKE, RKE, RNG *k-ε* and RSM were used for comparison using an unsteady solver. Table 3 shows the prediction errors of the static temperature in the PCL obtained using four different turbulence models. The results clearly showed that the RSM model yielded the lowest error (5.60%) compared to the other turbulence models. This may be attributed to the comprehensive turbulence modelling in RSM, which abandoned the assumption of isotropic turbulence, unlike in the *k-ε* based models. Turbulent flow is anisotropic in nature and hence, the RSM model is well suited for turbulence modelling (Fluent Inc, 2006; Gimbun, 2008). The SKE, RKE and RNG *k-ε* models give reasonable predictions, with errors of ranging from 5.86% to 7.04% due to the isotropic eddy viscosity assumption. This finding suggests that the RSM has the ability to accurately predict the turbulent flow in a PCL.

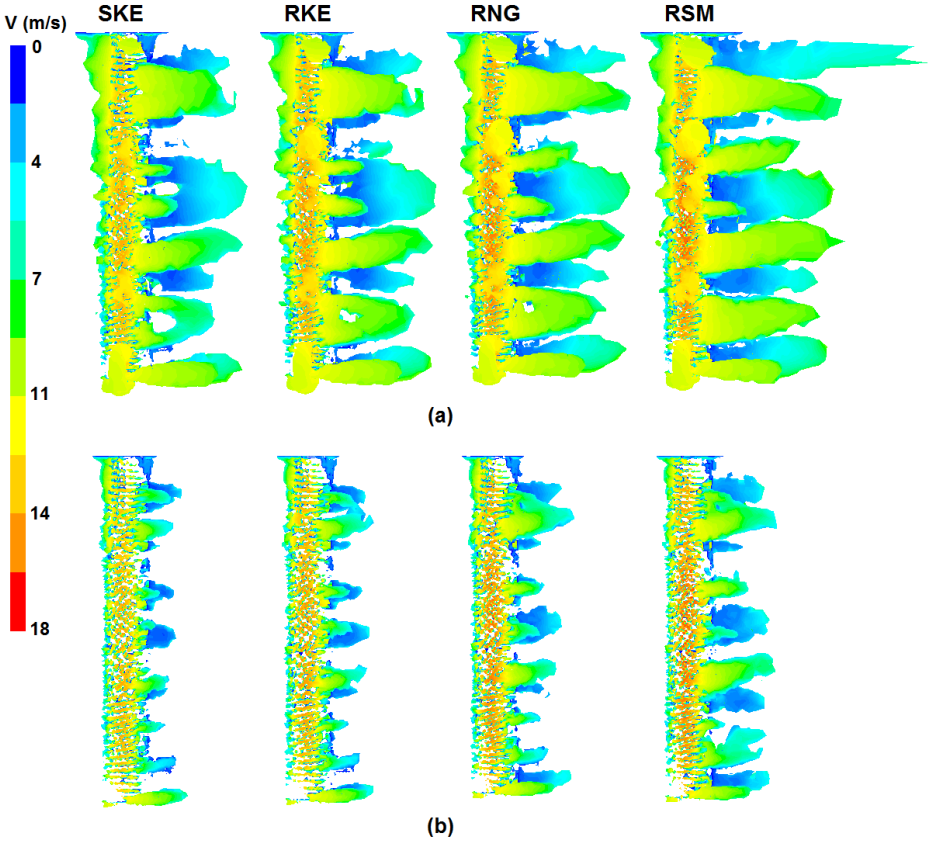

Fig. 3 - Turbulent structure coloured by velocity magnitude for four turbulent models using lambda-2 criterion at (a) λ_2 = -400; and (b) λ_2 = -5000.

Table 3 – Prediction accuracy of predicted static temperature at X = 5.85 m by different solver and turbulence models.

Case	Temperature (K)	Prediction error (%)
Experiment	1293.0	-
SKE (Steady)	1217.3	5.86 ± 0.09
SKE (Unsteady)	1217.3	5.86 ± 0.04
RKE (Unsteady)	1202.0	7.04 ± 0.00
RNG (Unsteady)	1204.8	6.82 ± 0.01
RSM (Unsteady)	1220.6	5.60 ± 0.01

The predicted combustion temperature is within the range of the published data for combustion involving H_2, CO and CH_4, which is discussed in detail in the following section on the effect of nozzle design. The overall mass balance for all four different nozzle designs showed a nearly zero deviation of mass balance between the inlet and outlet flows, indicating a good convergence (see supplementary data). In a closed system like PCL, the combustion process increases the internal energy of the gas species. As a result, the temperature increased with pressure due to the conversion of kinetic energy to dynamic pressure. In this work, the total pressure on the original design of PCL increased from 0.643 kPa to 0.656 kPa (about 2%). All three modified nozzle designs showed a pressure drop ranging from 13% to 23% due to larger flow disturbance induced by the winged nozzle as opposed to the original wingless design. Nevertheless, the increase in the pressure drop is compensated by the improvement in combustion efficiency using the winged nozzle design as discussed in the following section.

5.2 Influence of nozzle design

The effect of the wing addition prior to the oxygen nozzle was studied by evaluating three different wing designs of a roughly similar cross-sectional area. The temperature profile was predicted along the radial position after the nozzle, 1.5 m from the PCL inlet, as shown in Fig. 4. The chemical reaction between the syngas and oxygen takes place in the upwind region of the nozzle. Therefore, the peak temperature was achieved at two combustion regions (-0.3 m < Y < -0.1 m and 0.1 m < Y < 0.3 m) and decreased towards the PCL wall, as shown in Figs. 4 and 5. The result indicated that the new nozzle design gave a better combustion performance (i.e., higher peak temperature and bigger flame) compared to the original design. Among the new designs, design A showed the best performance, providing the highest peak temperature at 3088.3 K (over 45% higher than the original design). This is due to the flow recirculation which enhanced the mixing of syngas and O_2 induced by the wing structure.

In this work, the partial combustion was performed in a closed system, whereby the combustion occurs in a control volume. In contrast, the open-air combustion occurs at a constant pressure since the volume of the system expands to the atmosphere. According to Borate (2010), the adiabatic flame temperature of an open-air combustion is approximately 450 K lower than that in a closed system. This is due to energy conversion at work as a result of volume expansion in an open-air combustion system. CH_4, H_2 and CO are three major components in the inlet gas. Theoretically, the maximum adiabatic flame temperature during combustion with air for CH_4, H_2 and CO is 2148 K, 2400 K and 2394 K, respectively (Dahiya and Ami Chand, 1987). The value is much higher in the case of combustion using pure oxygen, i.e., 3083 K and 3100 K for CH_4 and H_2, respectively. These adiabatic flame temperatures were measured in an open-air combustion condition. The adiabatic flame temperature in a closed system is greater than in an open-air combustion (Borate, 2010). The combustion was performed using a pure O_2 from the oxygen lance, but the inlet gas introduced to the PCL contains 12.6% of N_2. Therefore, this work is closely comparable to a combustion by air. The predicted flame temperature ranging from 2126.9 K to 3088.3 K achieved in this work is reasonable, since they fell between the theoretical value reported in the literature.

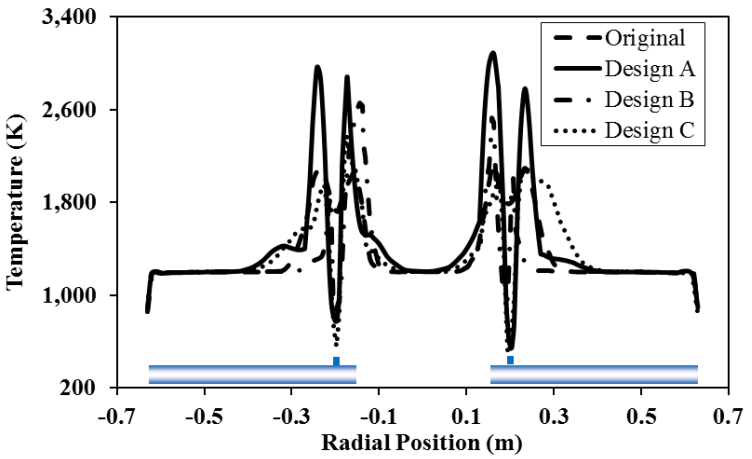

Fig. 4 - Predicted mean temperature profile for the four nozzle designs after the oxygen lances at X = 1.5 m.

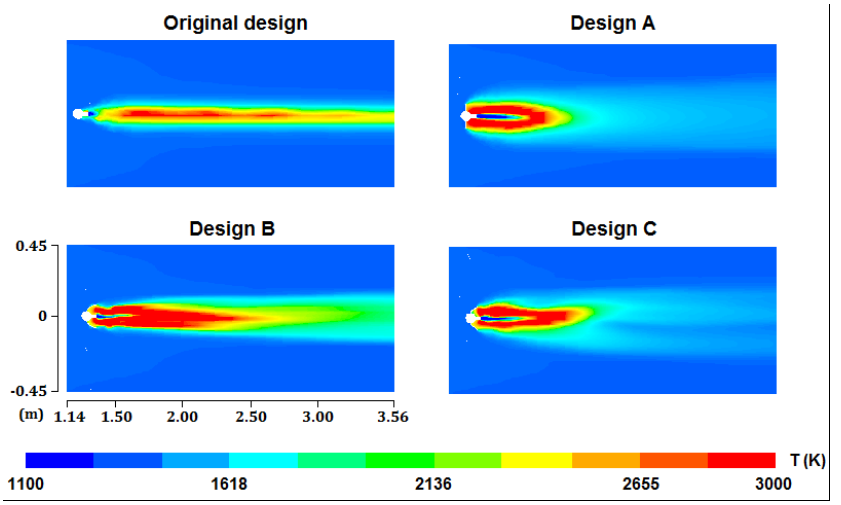

Fig. 5 - Contour plot of static temperature for the four different nozzle designs.

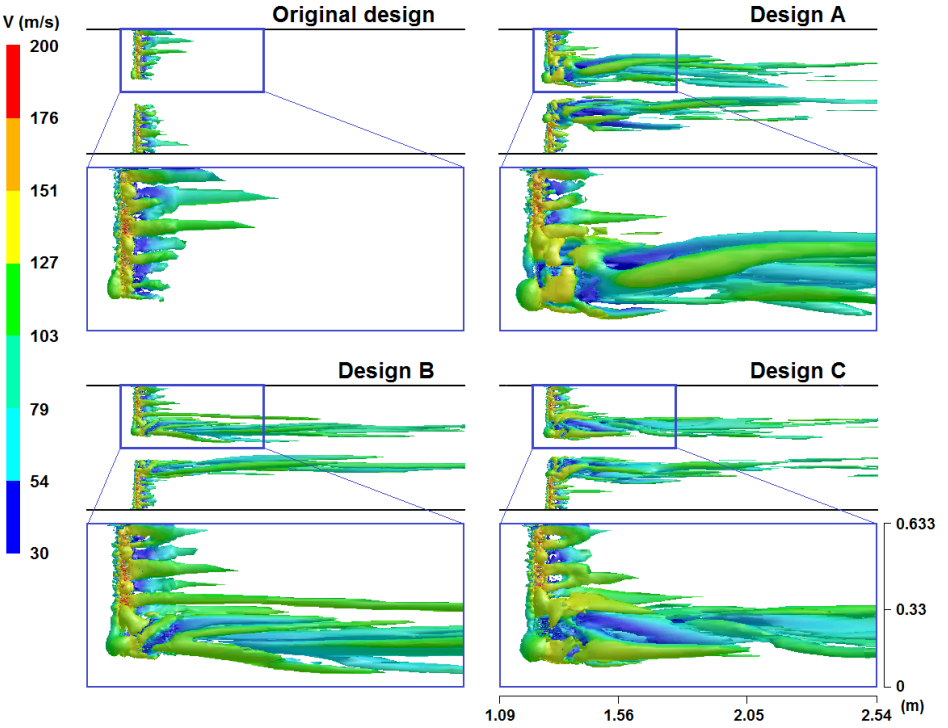

Fig. 6 - Turbulence structure coloured by velocity magnitude for the four nozzle designs using lambda-2 criterion at λ_2 = -30,000.

The partial combustion of syngas is part of the direct reduction process installed just before the oxide removal reactor. PCL is used to increase the temperature of syngas for the reduction process. The direct reduction process in a gas-solid reactor involves high temperature (more than 1193 K) and pressure (more than 55 kPa). High operating pressure reduces the product loss through the gas flow by increasing the mass flowrate of iron ore while keeping the velocity of syngas as low as possible. Therefore, the iron loss is minimised, increasing the reactor productivity. The plant productivity improves at higher operating temperature, but must be below the melting point of iron (1808.15 K) to avoid the sticking tendency of the iron ore during reduction. In this work, the outlet temperature (i.e., 1183.8 K, 1220.7 K, 1234.3 K and 1224.9 K for the original design, design A, B and C, respectively) is well below the

melting point of iron. The predicted temperature at the PCL wall of all four nozzle designs is below 1000 K (ranging from 847.3 to 966.9 K) which is considered safe, since it is much lower than the stainless steel melting point (1450 K).

Fig. 6 illustrates the instantaneous turbulence structure around the cylindrical oxygen lance for the four different nozzle designs. The iso-surface of velocity magnitude is represented by lambda-2 criterion at λ_2 = -30,000. A smaller-scale turbulent eddies is formed along the cylindrical oxygen lance away from the nozzle due to the flow disturbance, while larger laminar eddies is produced after the oxygen lance, as shown in Fig. 6. The modified winged nozzle induced stronger vortices compared to the original wingless design. The stronger flow disturbance enhanced the gas mixing and the reaction, resulting in a higher peak combustion temperature for all the modified nozzles.

The predicted turbulent kinetic energy at Y = 0.2 m from the PCL wall along the axial position is shown in Fig. 7. The oxygen lance is located at 1.35 m from the PCL inlet, and the nozzle is located about 0.2 m from the centre line of PCL. Fig. 7 showed a very low turbulent kinetic energy in the undisturbed flow region before the oxygen lance (0 m < X < 1.2 m). The highest predicted kinetic energy was achieved in the region just after the oxygen lance (1.35 m < X < 2.5 m) for the four nozzle designs. The attached wing is designed to facilitate the turbulence-induced mixing between the syngas and oxygen, thereby increasing the reaction rates of the combustion processes. Design A produced the highest turbulent kinetic energy, whereas the wingless design in the original PCL design showed a lower turbulent kinetic energy, as shown in Figs. 7 and 8. In fact, all of the proposed winged nozzle designs had a much higher turbulent kinetic energy compared to the original design due to the disturbance of flow by the wings. The fluid pathlines for the four different nozzle designs were shown in Fig. 9. Design A has a 90° angle to the direction of the flow and hence produced the largest flow disturbance. In contrast, design B and C have a curved edge facing the direction of the flow, resulting in less intense turbulence. Fig. 10 shows a comparison of the predicted turbulent dissipation rate of four different nozzle designs at axial position. During partial combustion, energy transferred from the larger eddies to smaller eddies. The larger eddies are responsible for turbulent kinetic energy, whereas the smaller ones are responsible for the turbulent dissipation rate. The kinetic energy may also be released as heat, which explains why the highest peak temperature was obtained from design A. The turbulent dissipation rate distribution for the four different nozzle designs at X = 1.5 m from the PCL inlet is shown in Fig. 11.

Figs. 12 and 13 show the axial velocity profiles at axial position and radial position, respectively. The highest axial velocity was achieved in the undisturbed flow before the oxygen lance (0 m < X < 1.3 m) at axial position and around the centre region (-0.1 m < Y < 0.1 m) at radial position. Whereas, the lowest axial velocities were observed behind the nozzle wing and in the combustion region, except for the original design (Figs. 9, 12 and 13). The wing induced a recirculation zone in the combustion region, which increased residence time, promoted mixing and enhanced combustion. A sufficiently higher residence time enhanced the chemical reaction, resulting a larger flame

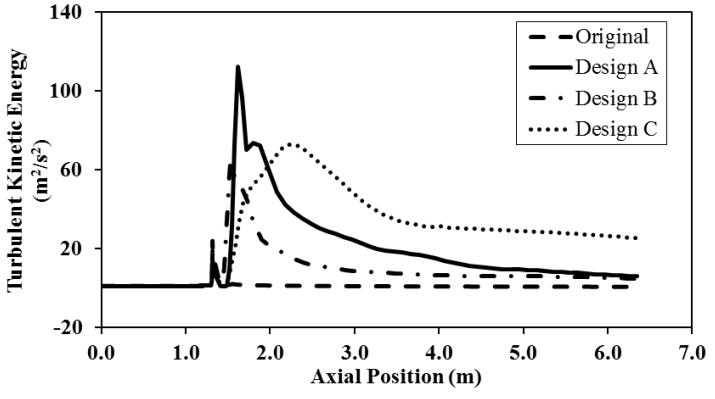

Fig. 7 - Turbulent kinetic energy prediction for the four nozzle designs at Y = 0.2 m from the PCL wall.

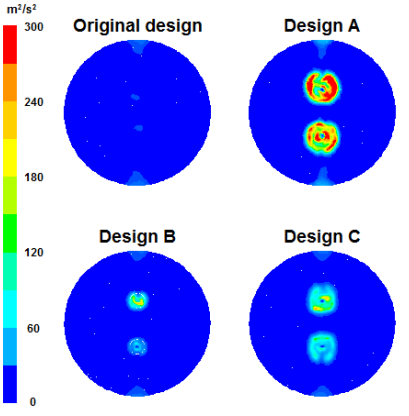

Fig. 8 - Turbulent kinetic energy distribution for the four nozzle designs after the oxygen lances at X = 1.5 m.

as reflected in the temperature contour (Fig. 5). In contrast, the axial velocity around the combustion region (-0.3 m < Y < -0.1 m and 0.1 m < Y < 0.3 m) of the original wingless nozzle design is much higher than the three modified nozzle designs. This forced the reaction to occur in a narrow region near the nozzle upwind direction, which prolonged the completion of the reaction as indicated by a slender and longer flame.

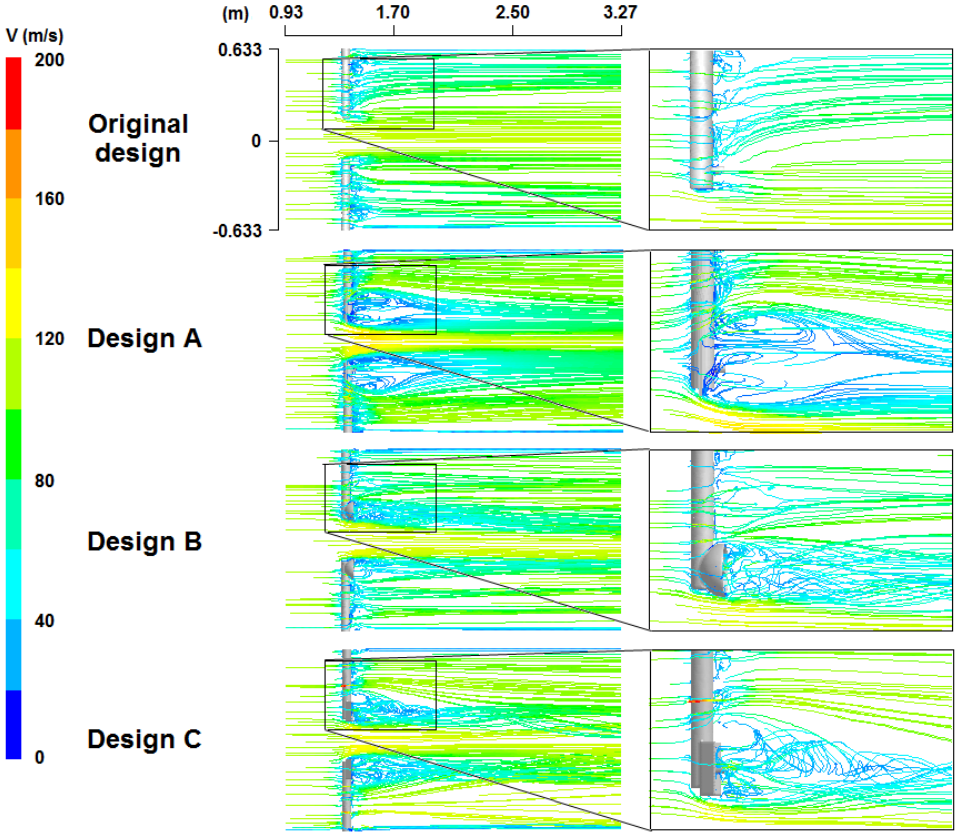

Fig. 9 - Fluid pathlines coloured by velocity magnitude of the four nozzle designs.

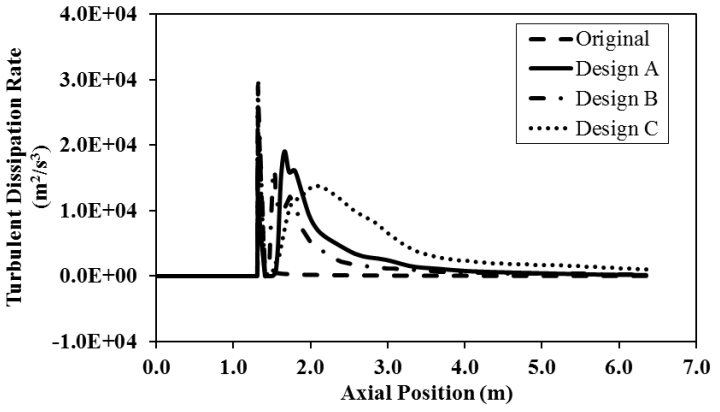

Fig. 10 - Turbulent dissipation rate prediction for the four nozzle designs at Y = 0.2 m from the PCL wall.

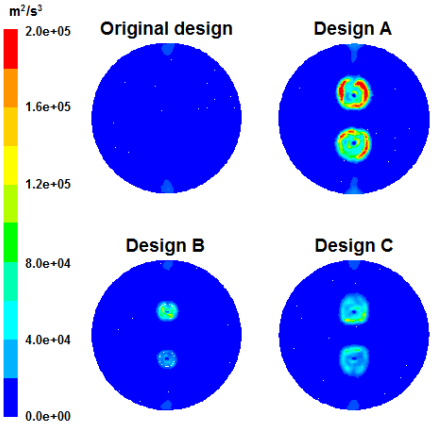

Fig. 11 - Turbulent dissipation rate distribution for the four nozzle designs after the oxygen lances at X = 1.5 m.

Fig. 14 shows the contour plots for five chemical reactions in the PCL. Combustion of syngas, which is composed of CO and H_2 (reactions 2 and 3) have much higher reaction rates than that of CH_4 (reactions 1 and 4), as shown in Fig. 14. The lower reaction intensity of CH_4 may also be attributed to the lower proportion of CH_4 in the inlet gas (13.2%). Incomplete and high-temperature reactions will lead to favourable conditions for CO formation. It is understood that the dissociation of CO_2 into CO and O_2 increases with temperature, especially above 1800 K (Nigara and Cales, 1986). This explained the highest rates of reaction 5 in this work with the modified nozzle design, which has significantly higher temperatures than the original design (Fig. 5). Combustion in a PCL is affected by turbulent mixing between the inlet gas and O_2 from the nozzle. Greater turbulent mixing between the species induces intense chemical reactions, resulting in higher flame intensity. The highest peak combustion temperature and largest flame were achieved by adding a flat wing (Design A) to the original design.

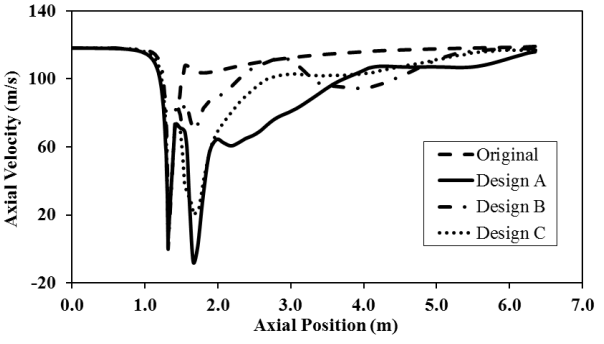

Fig. 12 - Axial velocity prediction for the four nozzle designs at Y = 0.2 m from the PCL wall.

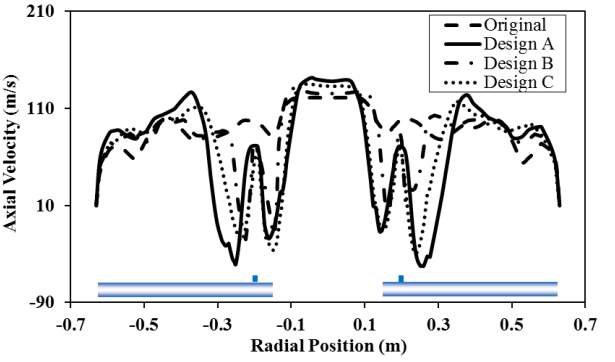

Fig. 13 - Axial velocity prediction for the four nozzle designs after the oxygen lances at X = 1.5 m.

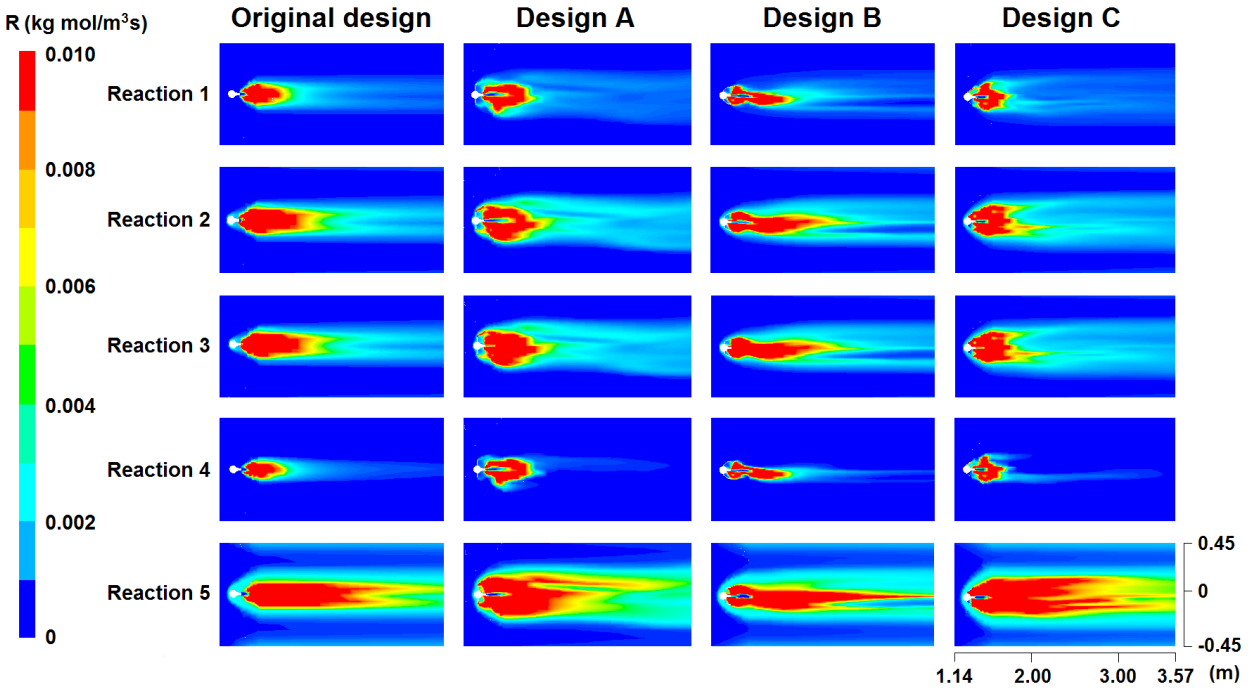

Fig. 14 - Contour plot of reaction rates obtained using the four nozzle designs.

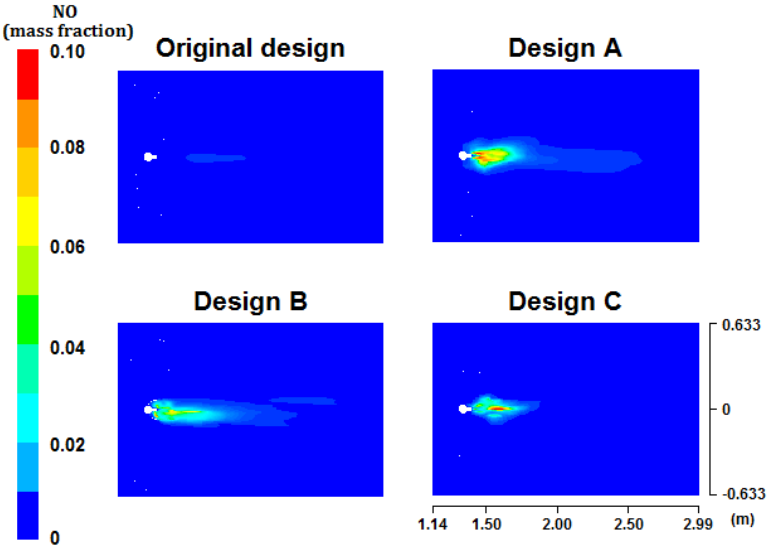

Fig. 15 - Contour plot of mass fraction of NO for the four nozzle designs after the oxygen lances at X = 1.5 m.

Nitrogen oxides (NO) formation is common for partial combustion process due to the presence of N_2 in the fuel gas and extremely high temperature. The formation of thermal NO is likely to occur at temperature above 1800 K (Fluent Inc, 2006). In this work, the thermal NO is the dominant process due to high temperature (above 1800 K) condition. The thermal NO in this work is mainly formed in the combustion region (1.2 m < X < 2.0 m) after the oxygen lance, shown in Fig. 15. However, only a trace concentration of NO was present at the outlet of the PCL, as the high-temperature region is confined to the small area just after the nozzle. The mass fraction of NO at the outlet were 0.0001%, 0.010%, 0.005% and 0.006% for the original design, design A, B and C, respectively (see supplementary data).

6. Conclusions

A suitable modelling strategy was successfully developed for a PCL using computational fluid dynamics. The best prediction was obtained using a combination of an unsteady solver with a second-order upwind scheme, standard pressure interpolation scheme and RSM turbulence model, with an error of approximately 6% from the measured combustion temperature. The new nozzle design showed a significant improvement in the PCL combustion, with over a peak temperature 45% higher than the original design. The highest peak combustion temperature was achieved by adding a flat wing (Design A) compared to the original oxygen nozzle design. Modified nozzle designs yielded a better syngas-oxygen mixing and combustion reaction, resulting in higher temperature of syngas which may improve the productivity of the steel manufacturing plant. The CFD model in this work can serve as a tool to evaluate the design of PCLs or for design retrofitting of an existing PCL since the effects of the design changes can be quickly evaluated.

Acknowledgements

W.P. Law thanks Ministry of Education Malaysia for the MyMaster scholarship. We acknowledge funding from Universiti Malaysia Pahang through GRS140331 and for provision of a PhD scholarship via Graduate Research Scheme.

References

Abbasi Khazaei, K., Hamidi, A.A., Rahimi, M., 2010. CFD modeling study of high temperature and low oxygen content exhaust gases combustion furnace. Iran. J. Chem. Chem. Eng. 29, 85-104.

Andersson, B., Andersson, R., Hakansson, L., Mortensen, M., Sudiyo, R., Wachem, B.V., 2012. Computational

Fluid Dynamics for Engineers. Cambridge University Press, New York.
Athayde, M., Nunes, S.F. Silva, G.A.L., 2012. Novel burner design supported by CFD to minimize deposits inside combustion chambers of samarco pelletizing furnaces. 6th International Congress on the Science and Technology of Ironmaking 2012 (ICSTI), Rio de Janeiro, Brazil.
Barik, A.K., Dash, S.K., Guha, A., 2015. Entrainment of air into an infrared suppression (IRS) device using circular and non-circular multiple nozzles. Comput. Fluids 114, 26-38.
Beaudan, P., Moin, P., 1994. Numerical experiments on the flow past a circular cylinder at sub-critical Reynolds number. Technical Report TF-62, Department of Mechanical Engineering, Stanford University, California.
Benajes, J., Pastor, J.V., Payri, R., Plazas, A.H., 2004. Analysis of the influence of diesel nozzle geometry in the injection rate characteristic. J. Fluids Eng. 126, 63–71.
Benim, A.C., Cagan, M., Gunes, D., 2004. Computational analysis of transient heat transfer in turbulent pipe. Int. J. Therm. Sci. 43, 725-732.
Borate, N.S., 2010. Flame temperature analysis and NOx emissions for different fuels. Michigan Technological University. Retrieved on 24 Sept 2014 from: www.chem.mtu.edu/~jmkeith/fuel_cell_curriculum/me_mods/ME_Combustion_And_Air_Pollution_Module_1.doc.
Bradley, D., Hundy, G.F., 1971. Burning velocities of methane-air mixtures using hot-wire anemometers in closed-vessel explosions. Symp. (Int.) Combust. 13, 575-583.
Brett, J., Tang, L., Hutchins, N., Valiyff, A., Ooi, A., 2010. Computational fluid dynamics analysis of the 1303 unmanned combat air vehicle. 17th Australasian Fluid Mechanics Conference, Auckland, New Zealand, 5-9 December 2010.
Dahiya, R.P., Ami Chand, 1987. Utilisation of hydrogen for domestic, commercial and industrial applications, in: Dahiya, R.P. (Eds.), Progress in Hydrogen Energy. Springer, Netherlands, pp. 179-194.
Fluent Inc., 2006. FLUENT 6.3 User's Guide. Lebanon, New Hampshire.
Galletti, C., Parente, A., Tognotti, L., 2007. Numerical and experimental investigation of a mild combustion burner. Combust. Flame 151, 649-664.
Gao, J., Moon, S., Zhang, Y., Nishida, K., Matsumoto, T., 2009. Flame structure of wall-impinging diesel fuel sprays injected by group-hole nozzles. Combust. Flame 156, 1263-1277.
Gimbun, J., Chuah, T.G., Fakhru'l-Razi, A., Choong, T.S., 2005. The influence of temperature and inlet velocity on cyclone pressure drop: a CFD study. Chem. Eng. Process. 44, 7-12.
Gimbun, J., 2008. CFD simulation of aerocyclone hydrodynamics and performance at extreme temperature. Eng. Appl. Comput. Fluid Mech. 2, 22-29.
Gimbun, J., Muhammad, N.I.S., Law, W.P., 2015. Fluid dynamics and transport phenomena unsteady RANS and detached eddy simulation of the multiphase flow in a co-current spray drying. Chin. J. Chem. Eng. In-press: doi:10.1016/j.cjche.2015.05.007.
Gubba, S.R., Ingham, D.B., Larsen, K.J., Ma, L., Pourkashanian, M., Tan, H.Z., Williams, A., Zhou, H., 2012. Numerical modelling of the co-firing of pulverized coal and straw in a 300 MWe tangentially fired boiler. Fuel Process. Technol. 104, 181-188.
Guessab, A., Aris, A., Bounif, A., 2013. Simulation of turbulent piloted methane non-premixed flame based on combination of finite-rate/eddy-dissipation model. MECHANIKA 19, 657-664.
Gulati, P., Katti, V., Prabhu, S.V., 2009. Influence of the shape of the nozzle on local heat transfer distribution between smooth flat surface and impinging air jet. Int. J. Therm. Sci. 48, 602-617.
Iaccarino, G., Ooi, A., Durbin, P.A., Behnia, M., 2003. Reynolds averaged simulation of unsteady separated flow. Int. J. Heat Fluid Flow 24, 147-156.
Incropera, F.P., DeWitt, D.P., 2000. Fundamentals of Heat and Mass Transfer, fourth ed. Wiley, New York.
Kazakidi, A., Tsakiris, D.P., Angelidis, D., Sotiropoulos, F., Ekaterinaris, J.A., 2015. CFD study of aquatic thrust generation by an octopus-like arm under intense prescribed deformations. Comput. Fluids 115, 54-65.
Keenan, J.H., Chao, J., Kaye, J., 1983. Gas Tables, John Wiley & Sons, New York.
Kravchenko, A.G., Moin, P., 2000. Numerical studies of flow over a circular cylinder at ReD=3900. Phys. Fluids 12, 403-417.
Law, W.P., Gimbun, J., 2015. A CFD study of a partial combustion lance. JESTEC 3, 68-78.
Lian, C., Merkle, C.L., 2011. Contrast between steady and time-averaged unsteady combustion simulations. Comput. Fluids 44, 328-338.

Lourenco, L.M., Shih, C., 1993. Characteristics of the plane turbulent near wake of a circular cylinder: A particle image velocity study (private communication), reported by Kravchenko, A.G., Moin, P., 2000. Numerical studies of flow over a circular cylinder at Re_D=3900, Phys. Fluids, 12, 403-417.

Magnussen, B.F., Hjertager, B.H., 1977. On mathematical modelling of turbulent combustion with species emphasis on soot formation and combustion. 16th Symposium (International) on Combustion. The Combustion Institute, Pittsburgh, 16, 719-729.

Miller, C.D., Olsen, H.L., Logan, W.O., Osterstrom, G.E., 1946. Analysis of spark-ignition engine knock as seen in photographs taken at 200,000 frames per second. NACA Report No. 857, Aircraft Engine Research Laboratory, 363-373.

Muddada, S., Patnaik, B.S.V., 2010. An assessment of turbulence models for the prediction of flow past a circular cylinder with momentum injection. J. Wind Eng. Ind. Aerodyn. 98, 575-591.

Nicolle, J., Labbe, P., Gauthier, G., Lussier, M., 2010. Impact of blade geometry differences for the CFD performance analysis of existing turbines. 25th IAHR Symposium on Hydraulic Mahinery and Systems. IOP Conference Series: Earth and Environmental Science 12, 012028.

Nigara, Y., Cales, B., 1986. Production of carbon monoxide by direct thermal splitting of carbon dioxide at high temperature. Bull. Chem. Soc. Jpn. 59, 1997-2002.

Park, S., Kim, J.A., Ryu, C., Chae, T., Yang, W., Kim, Y.J., Park, H.Y., Lim, H.C., 2013. Combustion and heat transfer characteristics of oxy-coal combustion in a 100 MWe front-wall-fired furnace. Fuel 106, 718-729.

Piomelli, U., 2014. Large eddy simulation in 2030 and beyond. Phil. Trans. R. Soc. 372, 1-13. doi: 10.1098/rsta.2013.0320.

Rodi, W., 1997. Comparison of LES and RANS calculations of the flow around bluff bodies. J. Wind Eng. Ind. Aerodyn. 69-71, 55-75.

Shih, T.H., Liou, W.W., Shabbir, A., Yang, Z., Zhu, J., 1995. A new k-ε eddy viscosity model for high Reynolds number turbulent flows. Comput. Fluids 24, 227-238.

Sieder, E.N., Tate, G.E., 1936. Heat transfer and pressure drop of liquids in tubes. Ind. Eng. Chem. 28, 1429-1435.

Som, S., Ramirez, A.I., Longman, D.E., Aggarwal, S.K., 2011. Effect of nozzle orifice geometry on spray, combustion, and emission characteristics under diesel engine conditions. Fuel 90, 1267–1276.

Taskiran, O.O., Ergeneman, M., 2014. Effect of nozzle dimensions and fuel type on flame lift-off length. Fuel 115, 833-840.

Touloukian, Y.S., Liley, P.E., Saxena, S.C., 1970a. Thermophysical Properties of Matter: Thermal Conductivity, vol. 3. IFI/Plenum, New York.

Touloukian, Y.S., Saxena, S.C., Hestermans, P., 1970b. Thermophysical Properties of Matter: Viscosity, vol. 11. IFI/Plenum, New York.

Unal, U.O., Atlar, M., Goren, O., 2010. Effect of turbulence modelling on the computation of the near-wake flow of a circular cylinder. Ocean Eng. 37, 387-399.

Welty, J.R., Wicks, C.E., Wilson, R.E., Rorrer, G., 2001. Fundamentals of Momentum, Heat, and Mass Transfer, fourth ed. John Wiley & Sons, New York.

Westbrook, C. K., & Dryer, F. L. (1984). Chemical kinetic modeling of hydrocarbon combustion. Progress in Energy and Combustion Science 10 (1), 1-57.

Yakhot, V., Orszag, S.A., 1986. Renormalization group analysis of turbulence I: Basic theory. J. Sci. Comput. 1, 3-51.

Zain, M.I.S., Gimbun, J., Hassan, Z., 2011. CFD study on the performance of oxygen lance for partial combustion unit at direct reduction plant. International Conference on Chemical Innovation 2011, International Training Centre, TATI University College, Terengganu.

Zhang, Z., Zhao, C., Xie, Z., Zhang, F., Zhao, Z., 2014a. Study on the effect of the nozzle diameter and swirl ratio on the combustion process for an opposed-piston two-stroke diesel engine. Energy Procedia 61, 542-546.

Zhang, Y.W., Bo, Y., Wu, Y.C., Wu, X.C., Huang, Z.Y., Zhou, J.H., Cen, K.F., 2014b. Flow behavior of high-temperature flue gas in the heat transfer chamber of a pilot-scale coal-water slurry combustion furnace. Particuology 17, 114-124.